frontiers | Frontiers in Energy Research

TYPE Original Research
PUBLISHED 01 May 2024
DOI 10.3389/fenrg.2024.1386538

OPEN ACCESS

EDITED BY
Sanjeev K. Sharma,
Chaudhary Charan Singh University, India

REVIEWED BY
Viswanathan S. Saji,
Interdisciplinary Research Center for Advanced Materials, Saudi Arabia
Gaurav Sharma,
Indian Institute of Technology Delhi, India

*CORRESPONDENCE
Dandan Yin,
aayindan@163.com

RECEIVED 15 February 2024
ACCEPTED 04 April 2024
PUBLISHED 01 May 2024

CITATION
Yin D, Li Q, Zhao D and Huang T (2024), Modified silica nanoparticles stabilized foam for enhanced oil recovery.
Front. Energy Res. 12:1386538.
doi: 10.3389/fenrg.2024.1386538

Modified silica nanoparticles stabilized foam for enhanced oil recovery

Dandan Yin*, Qiuzi Li, Dongfeng Zhao and Tao Huang

College of Petrochemical Engineering and Environment, Zhejiang Ocean University, Zhoushan, China

Foam has been successfully used to improve mobility control in the process of enhanced oil recovery, yet the instability of foam limits its application. Modified nanoparticles with varying wettability were prepared by reacting 3-methacryloxypropyltrimethoxysilane (KH570) with spherical SiO_2 nanoparticles in this study. Fourier transform infrared (FTIR) spectra and the measured contact angles were used to characterize the surface properties of the modified SiO_2 particles, and the foam stabilization effects of wettability SiO_2 were compared. Pore-scale visualization experiments were conducted using a 2D micromodel to identify the prevailing enhanced oil recovery (EOR) mechanisms of modified nano SiO_2-Sodium alpha-olefin Sulfonate (AOS) foam flooding. The results indicate that modified SiO_2 effectively improves foam stability by adsorbing on the bubble surface and forming a mesh-like structure. The optimum contact angle of the particles is approximately 60°, resulting in a significant increase in drainage half-life by 29.4% compared to foam stabilized only by AOS. Additionally, Foam stabilized by modified SiO_2 demonstrates superior dynamic stability and deformation resistance. The modified SiO_2 stabilized foam exhibits enhanced interfacial viscoelasticity and plugging and profile control performance, surpassing AOS foam in displacing more residual oil in dead-end pores. The oil recovery of the micro model was determined by ImageJ software. KH570@ SiO_2 (0.2wt%)-AOS (0.2wt%) foam flooding increased the recovery by 8.7% compared to AOS (0.2wt%) foam flooding.

KEYWORDS

foam stability, SiO_2 nanoparticles, surface modification, profile control, enhanced oil recovery

1 Introduction

Foam flooding has been established as an effective method for enhancing the oil recovery of heterogeneous oil reservoirs (Li et al., 2008; Farajzadeh et al., 2010). Water flooding, a widely used and cost-effective technique, typically displaces only 30%–50% of the original oil in reservoirs (Yao et al., 2012; Wang et al., 2013). During water flooding, the water tends to flow into high-permeability layers, however, most low-permeability layers cannot be displaced (Xie et al., 2007). In addition, water may bypass flow due to the high viscosity ratio between oil and water. Foam fluid is a compressible non-Newtonian fluid with a selective seepage in the micropore paths. Foam will plug high-permeability layers, redirecting subsequent fluid flow toward low-permeability layers (Sun et al., 2014; Shi et al., 2023). Nonetheless, the thermodynamic instability of foam is a critical factor influencing its application (Sun et al., 2015; Almubarak et al., 2020). To address this issue, surfactants and polymers are commonly employed to stabilize foam (Mingming and Shuzhong, 2014; Wang

and Li, 2016). Polymers increase the viscosity of the liquid film, thereby increasing resistance to gas diffusion and stabilizing foam (Wang, 2014). Surfactants create a dense adsorption layer on the liquid film, diminishing the effective permeability of gas and bolstering surface elasticity, thereby inhibiting foam coalescence rates (Khristov et al., 1983; Pozrikidis, 2001). However, polymers and surfactants are susceptible to degradation in subsurface rock and may suffer from retention, ultimately escalating costs (Wang et al., 2020). In recent years, nanoparticles (NPs) have emerged as a promising novel foam stabilizer (Zhao et al., 2021). The adsorption of NPs at the gas-liquid interface is a thermodynamically spontaneous process capable of reducing the system's energy (Pieranski, 1980). Additionally, NPs adsorbed at the interface can form a solid-like structure, effectively restraining foam coalescence and enhancing foam stability (Bizmark and Ioannidis, 2018; Rezaee et al., 2022). Compared to traditional stabilizers like surfactants or thickeners, NPs are deemed exceptional interfacial modifiers due to their minimal toxicity to humans and environmentally friendly (Linke and Drusch, 2018; Deschamps et al., 2019; Qi et al., 2021). Furthermore, NPs exhibit minimal retention in porous media (Maestro et al., 2014; Khajehpour et al., 2018). Nanoparticles enhance the properties of the foam and optimize its resistance to high temperature and pressure (Ojea-Jiménez et al., 2016; Gu et al., 2022). Remarkably, NPs can traverse through pores and throats in rocks without causing pore plugging, so NPs can adapt to harsh formation environments (Horozov, 2008; Hu et al., 2023; Khandoozi et al., 2023).

SiO_2 nanoparticles (SNPs) have been used extensively in many fields due to their unique properties. Ordinary SNPs with a hydroxyl group (-OH) content exceeding 70% on the surface exhibit high hydrophilicity. However, neither excessive hydrophilicity nor hydrophobicity of SNPs can adsorb firmly at the gas-liquid interface, so they cannot stabilize the bubble well. The desorption energy of SNPs and the maximum capillary pressure they can form is closely related to the contact angle, underscoring the significance of achieving an optimal contact angle for effective foam stabilization (So and Lumsdon, 2000; Binks and Horozov, 2005). The formulation of nanofluids for foam generation stabilization was investigated by many researchers. Various surfactants such as cetyltrimethylammonium bromide (CTAB) and sodium dodecyl sulfate (SDS) have been employed through physical adsorption methods (Santini et al., 2011), However, the efficacy of these surface modifications is limited. Recognizing this limitation, silane coupling agents have emerged as widely utilized chemical modifiers for SNPs (Zhu et al., 2017). Some studies have explored adjusting the dosage of dichloro dimethyl silane (KH550) to alter the surface wettability of SNPs, resulting in modified particles with Si-OH group content (32%) and exhibiting favorable hydrophobic effects, characterized by an optimal contact angle ranging from 50° to 90° (Kaptay, 2003; Yousef et al., 2017). Hunter (Hunter et al., 2009) suggested that SNPs with contact angles between 60° and 70° serve as optimal foam stabilizers. Despite the recognized importance of hydrophobicity for the foam stabilization ability of NPs (Sie and Nguyen, 2020), there remains a lack of consensus in existing research regarding the impact of hydrophobicity of SNPs on foam stability. Various experiments have existed to demonstrate the effectiveness of nano-stabilized foam in enhancing oil recovery. Singh and Mohanty investigated the synergistic interaction between surfactants and SNPs and their effect on foam stability in the presence or absence of oil. Core displacement experiments showed that SNPs-stabilized foam can increase the recovery by 34% compared to water injection (Singh and Mohanty, 2017). Zhao et al. (2021) demonstrated the synergistic effect of anionic surfactant/silica mixtures in improving CO_2 foam stability and enhancing heavy oil recovery through microscopic visualization experiments. Bayat et al. (2016) studied the effects of SiO_2, Al_2O_3, TiO_2, and CuO on the stability of CO_2 foam and concluded that SiO_2 and Al_2O_3 provided the highest recovery due to their superior stability. Du et al. (2022) reported the ability of QDs@SIL [magnetic quantum dots modified by silane-coupled ionic liquid (SIL)] to stabilize foam, resulting in increased pressure gradients and enhanced recovery. However, Previous studies focus on how much nanoparticle-stabilized foam enhances recovery in porous media, but there are few visual studies on the influence of modified nanoparticles on foam deformation, and there have been few substantive investigations into modified nanoparticles affecting the foam behavior within porous media. For the study of foam stabilized by modified nanoparticles, core displacement experiments or 2D models are also used to prove the effect of nanoparticles on oil recovery. The microscopic mechanism of the EOR of the foam stabilized by modified nanoparticles and surfactant is not clear enough. Although the priming effect on the same type of remaining oil is compared, the process and principle of starting the remaining oil are not presented.

To achieve this, KH570 reacts with spherical SNPs to reduce the hydrophilicity of the surface. Characterization of the modified SNPs involved analyzing their molecular structure, wettability, and dispersion in surfactant solutions using Fourier-transform infrared spectroscopy, contact angle measurements, and particle size analysis, respectively. The impact of the wettability of SNPs on foam stability was assessed by tracking parameters such as foam volume, drainage half-life, and foam particle size evolution over time. Additionally, microscopic displacement experiments were conducted to explore how nanoparticles adsorb at the gas-liquid interface influence foam flow and enhance oil recovery. Through this investigation, insights into the micro-flow characteristics and the underlying mechanisms of enhanced oil recovery in SNPs-stabilized foam were elucidated.

2 Materials and methods

2.1 Materials

Sodium alpha-olefin Sulfonate (AOS, C14–16) with a molecular weight of 315w, which was supplied by Sigma (United States), both with a purity of >99.0%. KH570 (CP) was from Sinopdrug Group Chemical Reagents Co., LTD. SiO_2 nanoparticles (HDK, H19), as a white powder, were supplied by Germany Wacker Chemical Co., Ltd. The average diameter of the SiO_2 particles is 15 nm, with a specific surface area (SSA) of 170–200 m^2/g and purity of over 99%. Distilled water was used in the following AOS and/or SiO_2 solution systems. Both the surfactant and SNPs were used as received without further purification. The crude oil obtained from the Daqing oil reservoir has a density of 0.8126 g/cm^3 and a viscosity of 7.69 mPa·s

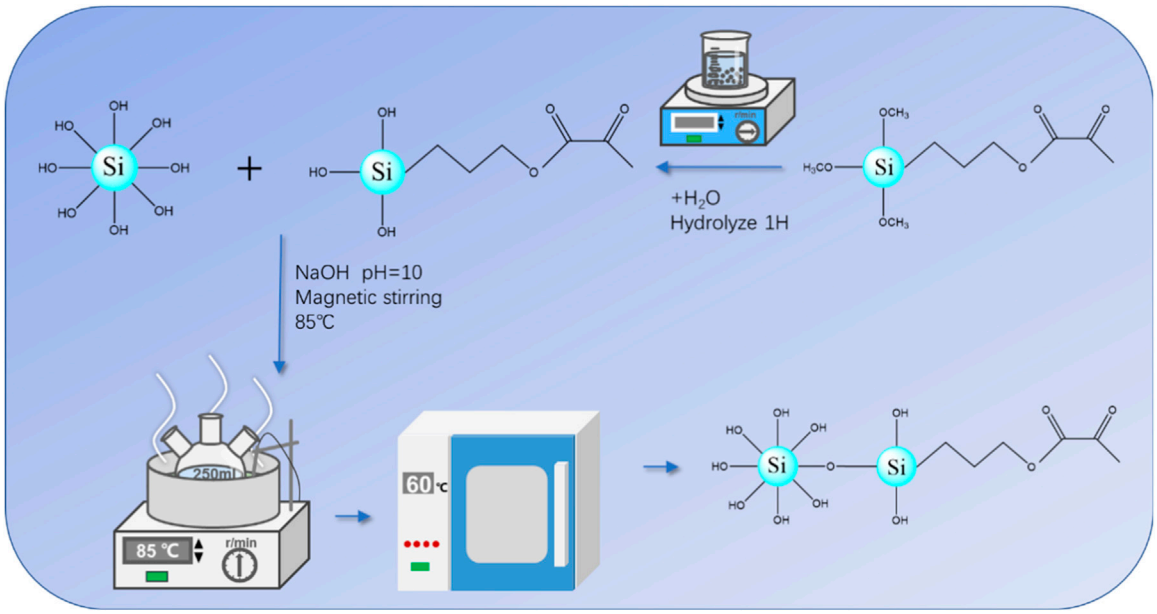

FIGURE 1
Schematic illustration of the synthetic route of KH570@SiO_2 nanoparticles.

at 25°C. NaOH (97%) was purchased from Chemiz China. Experiments were conducted at room temperature 25°C.

2.2 Methods

2.2.1 Modification of SiO_2 nanoparticles

The process begins with the reaction of the methoxy group (-CH_3O) from the silane coupling agent KH570 with water, resulting in the formation of silica hydroxyl (-Si-OH). The silica hydroxyl newly generated undergoes a dehydration condensation reaction with the silica hydroxyl groups on the SNPs, making the surface of the somewhat hydrophilic SNPs, as depicted in Figure 1. To initiate the synthesis, 1.0 g of SNPs is initially dispersed in 100 mL of anhydrous ethanol with the assistance of ultrasound for 10 min forming a dispersion, and this mixture was referred to as solution A. Different mass fractions of KH570 are added into a 50 mL ethanol solution (80 wt%) and hydrolyzed under magnetic stirring for 1 h, leading to the creation of solutions with varying concentrations of KH570, designated as solution B. Next, solution A is transferred into a 250 mL three-necked flask, followed by the adjustment of the pH to 9–10 using NaOH. While maintaining stirring at 85°C, solution B is added dropwise and continuously stirred, allowing the reaction to progress under reflux conditions for 4 h. After the completion of the reaction, the resulting product is washed with anhydrous ethanol and filtered until the filtrate becomes transparent. Subsequently, the product is dried in an oven at 60°C for 12 h and ground into a fine powder.

2.2.2 Characterization of SiO_2 nanoparticles

The surface functional groups of the SNPs were characterized using a Fourier-transform infrared spectrometer (FTIR, IRTracer-100) with a scanning resolution of 4 cm^{-1} both before and after modification. To determine the modification degree, SiO_2 was initially mixed with a specific amount of KBr, ground repeatedly, pressed, and subjected to infrared absorption intensity measurement. By comparing the absorption peak intensity with that of the original SNPs, the reduction in surface -OH was observed through the FTIR, aiding in assessing the extent of modification. The contact angle of KH570@SiO_2 was determined using a dynamic contact angle measurement system (Data physics OCA15EC) with each measurement performed thrice for reproducibility. Subsequently, KH570@SiO_2 or original SNPs were incorporated into the AOS solution and sonicated to create KH570@SiO_2-AOS or SiO_2-AOS dispersion systems, respectively. The particle size distribution of the dispersion system was then analyzed using a laser particle size analyzer (Malvern NS 90).

2.2.3 Foamability and foam stability

Bulk foam stability testing is often used as a fundamental screening tool to assess the foamability of diverse formulations of foam, despite variations in foam size between porous media and the free state (Singh et al., 2016). To evaluate foam stability, static foam stability experiments were conducted following the Waring blender method (Guo et al., 2006). Initially, various wettability of KH570@SiO_2 nanoparticles (0.2 wt%) were dispersed in a 200 mL AOS (0.2 wt%) solution utilizing an ultrasonic disperser to establish a dispersion system. The foam was then created by agitating the system in a blender (8,000 rpm) for 3 min and subsequently transferred to a graduated cylinder. Foamability and foam stability were assessed based on the initial foam volume (V_0) and the drainage half-life ($t_{1/2}$), representing the duration for half of the liquid to drain from the foam. Furthermore, a more detailed observation of the foam texture was achieved by dropping the lower foam layer onto a slide using a dropper, followed by covering it with a cover glass to create a single-layer distribution

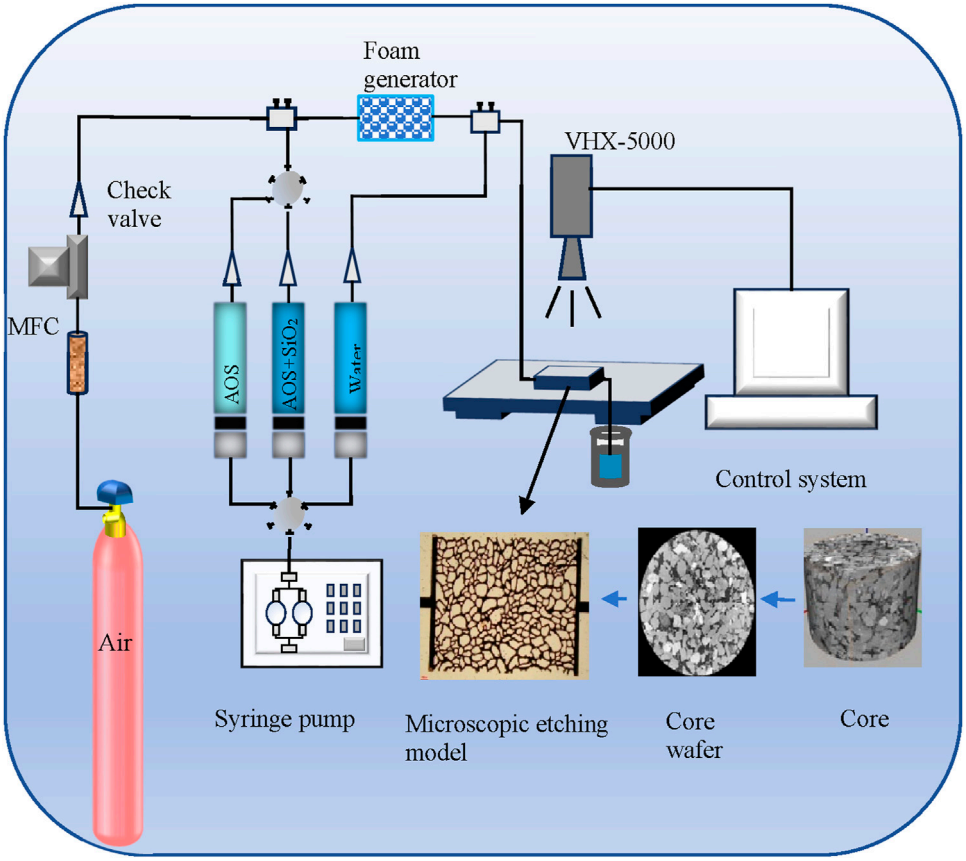

FIGURE 2
The flow diagram of the microscopic flooding experiment.

of foam. High-resolution three-dimensional super-depth microscopy (VHX-5000, Keyence) and a high-quality camera were used to capture the bubbles' shapes and diameters at different time points. The acquired images were analyzed using ImageJ software, which facilitated the calculation of the number and area of bubbles over time, along with determining the bubbles' diameters through image processing and statistical analysis.

2.2.4 Adsorption of particles on the foam surface

The adsorption of SNPs at the bubble surface and the mechanism of KH570@SiO_2-stabilized foam were investigated using fluorescence microscopy (Trim Scope, Germany). A fluorescent probe, Rhodamine B with a negative charge and a maximum excitation wavelength of 543 nm, was employed in this study. Initially, SNPs in the dispersion were stained with Rhodamine B, followed by centrifugation and washing with distilled water until the upper layer became clear. Subsequently, foam stabilized by the stained nanoparticles was prepared according to the standard procedure, enabling the collection of fluorescence images of the foam using a microscope.

2.2.5 Nanoparticle-stabilized foam flooding

A microscopic etched porous media model was made for foam flooding experiments. Through a photolithographic approach, a pore network resembling the real pore structure of natural cores from the Daqing oilfield was etched onto a glass plate. Upon sintering this etched glass plate with another smooth glass plate, the microscopic model was formed. The glass micro-model was designed with a porosity of 25%, featuring an average pore depth of approximately 40 μm and a width of 100 μm. Comprising three main components of the microscopic displacement device—the foam generation device, microscopic pore model, and observation/data collection device illustrated in Figure 2–the microscopic displacement apparatus was established. Initially, the microscopic model was evacuated, following which the pores were filled with crude oil (μ = 7.69 mPa·s, 25°C). The subsequent water flood involved injecting water for 10 pore volumes (PV) until no oil production occurred, signaling the termination of the water flooding phase and the beginning of the high-water saturation stage. Foam generation involved injecting foam solution and air into the foam generator at a 1:1 volume ratio, proceeding with a 2 PV injection for AOS foam or KH570@SiO_2-AOS stabilized foam. This was followed by an additional 5 PV of water flooding, with a consistent injection rate of 1 μL/min. Throughout the displacement process, an observation microscope (VHX-5000, Keyence) and a high-resolution CCD camera with a parallel light source documented the entire process. The study focused on investigating the effect of KH570@SiO_2-AOS stabilized foam flooding on the mobilization of various residual oils during the high-water saturation period, conducted at a temperature of 25°C. Microscopic displacement

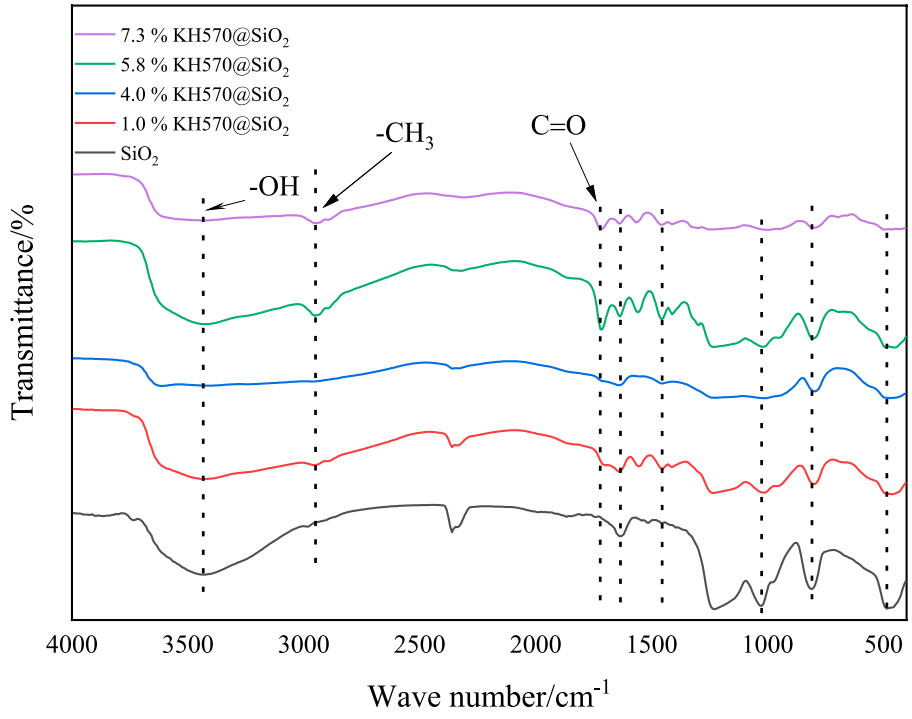

FIGURE 3
FTIR spectra of SNPs as a function of the KH570 concentration.

images were continuously recorded during the flooding experiment. To obtain the oil saturation from the remaining oil image, the image was sharpened to improve the contrast. Water and oil in the image were then distinguished based on a gray threshold according to a program developed in Python. Finally, the oil saturation was obtained by calculating the oil hole area ratio. Upon completion of the experiments, petroleum ether and ethanol were injected into the micro-model to clean all pore throats. Subsequently, the micro-model was placed in a constant-temperature oven at 45°C for drying.

3 Results and discussion

3.1 Surface properties of silica nanoparticles

3.1.1 Infrared spectrum analysis

The FTIR spectra of the SNPs are illustrated in Figure 3. In the spectrum of naked SNPs, the presence of -OH on the SiO_2 surface is indicated by the -OH peak observed in the range of 3,400–3,600 cm^{-1}. Even after modification, the persistence of -OH suggests that it did not completely react with the hydrolyzed KH570. The bending vibration of the O–H bond is represented by the absorption peak at 1,635 cm^{-1}. The characteristic peaks at 1,091 cm^{-1}, 810 cm^{-1}, and 486 cm^{-1} correspond to the asymmetric stretching vibration, symmetric stretching vibration, and bending vibration of the Si–O–Si bonds on the surface of SiO_2, indicating the presence of structural water on the K570@SiO_2 nanoparticles surface. The peak at 2,954 cm^{-1} is attributed to the asymmetric and symmetric stretching vibrations of the C-H bonds in $-CH_3$. Furthermore, the stretching vibration of the C=O bond is represented by the peak at 1718.21 cm^{-1}, while the peak at 1,234.44 cm^{-1} represents the stretching vibration of the C-O-C bond (Coates, 2000; Smith, 2018). These peaks suggest a reaction between the groups on the SiO_2 surface and KH570, leading to the successful coverage of the surface of the SNPs by $-CH_3$. As the KH570 content increases, the absorbance of the surface structured water at 3,200–3,600 cm^{-1} and the surface -OH at 1,636 cm^{-1} gradually weaken, indicating the grafting of KH570 onto the SNPs surface in the form of a Si–O–Si bond.

3.1.2 Hydrophobicity analysis

According to the above experiments, the organic hydrophobic groups were successfully grafted onto the surface of SNPs after modification. This grafting necessarily changes the surface hydrophobicity of the SNPs. Figure 4 illustrates the change in the contact angle of SiO_2 with the content of KH570. The initial contact angle on the surface of naked SNPs is in the range of 0°–15° (as in Figure 4A), where water dropped onto a SiO_2 thin film spreads and rapidly penetrates the substrate. The contact angle of SiO_2 first increases with the increase of KH570 content and then reaches a plateau, as in Figures 4B–H and Figure 5. This indicates that KH570 effectively alters the surface hydrophobicity of SiO_2. When the concentration of KH570 reaches 7.7%, the contact angle of SiO_2 reaches 91.2° as in Figure 4H. However, as the content of KH570 continues to increase, When the contact angle ranges from 30° to 80° does not continue to increase. This is because a self-condensation side reaction occurs between the hydrolysis products of KH570 and Si–OH. With an increase in KH570 content, both the grafting of silane alcohol with SNPs and the extent of the self-condensation reaction intensifies.

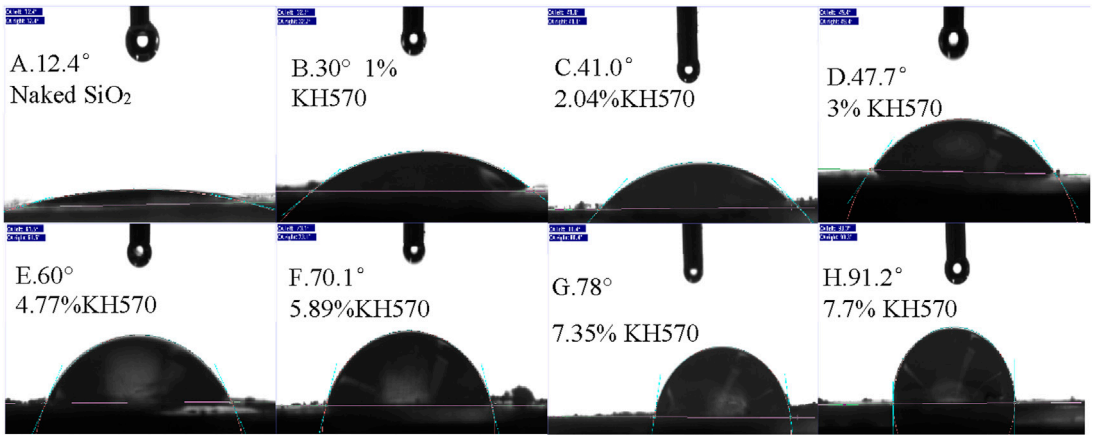

FIGURE 4
Contact angles images of KH570@SiO_2 nanoparticles.

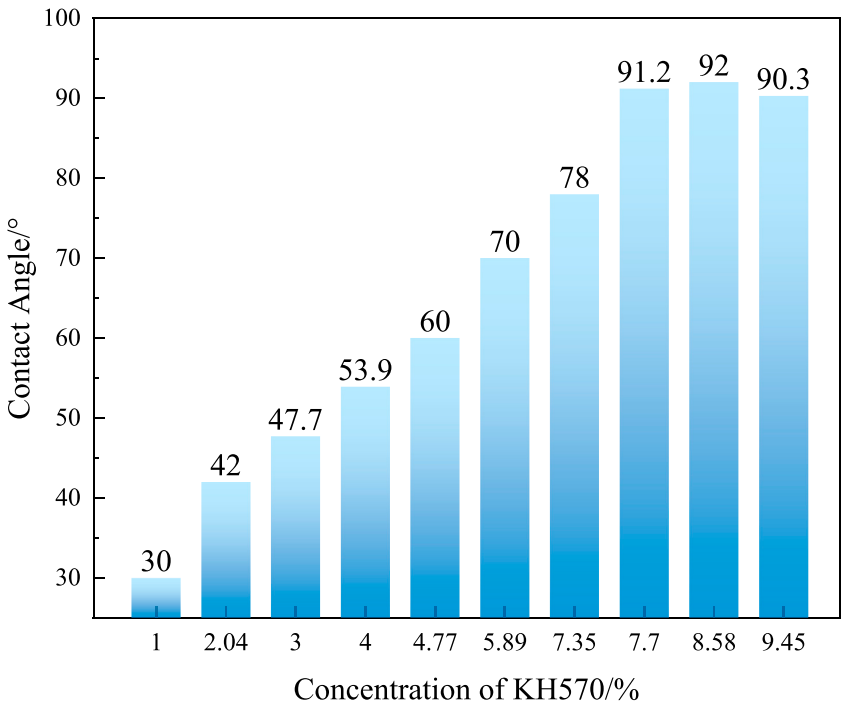

FIGURE 5
Contact angles of KH570@SiO_2 nanoparticles as a function of KH570 concentration.

However, when KH570 content is excessive, it tends to favor self-polymerization rather than grafting onto the surface of SNPs.

3.1.3 Dispersion of SNPs in AOS solution

In an AOS solution, a good foam stabilizer must be dispersed well. Figure 6 presents the median diameter (D_{50}) of the aggregation of SNPs (0.2wt%) in an AOS (0.2wt%) solution. The naked SNPs tend to cluster together, forming aggregates with a D_{50} of around 200 nm, which lose their nanoparticle properties. Conversely, the KH570@SiO_2 nanoparticles exhibit mitigated aggregation when the contact angle ranges from 30° to 80°, leading to an improvement in dispersion within the AOS solution as evidenced by a decrease in D_{50} to below 100 nm as the contact angle reaches 50°–60°. However, when the contact angle surpasses 80°, severe aggregation reoccurs, with the D_{50} exceeding 200 nm. This phenomenon is attributed to the heightened hydrophobicity that arises from the introduction of hydrophobic groups, thereby intensifying van der Waals forces between particles. The enhanced intermolecular interactions cause the particles to repel the aqueous phase, which ultimately results in their increased proximity and aggregation.

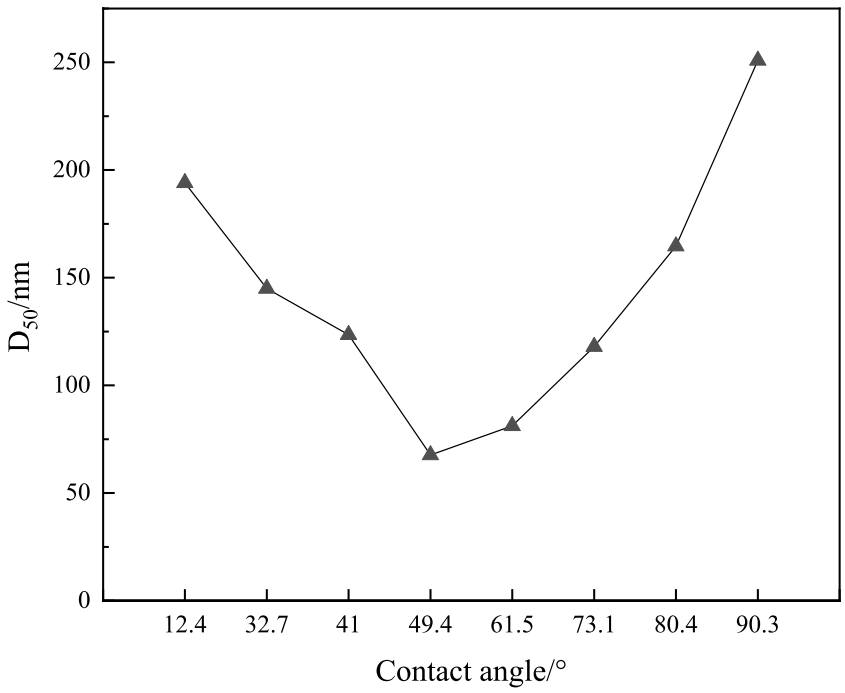

FIGURE 6
D_{50} of SiO_2/KH570@SiO_2 nanoparticles as a function of the Contact angles.

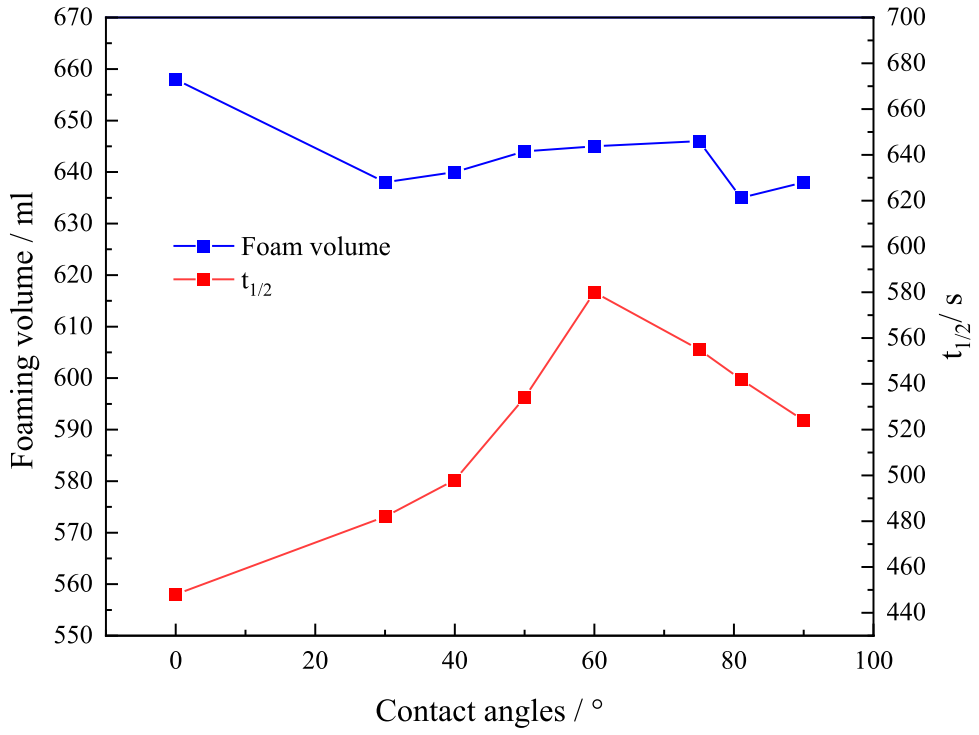

FIGURE 7
Stability and volumes of foam stabilized by KH570@SiO_2 with different contact angles.

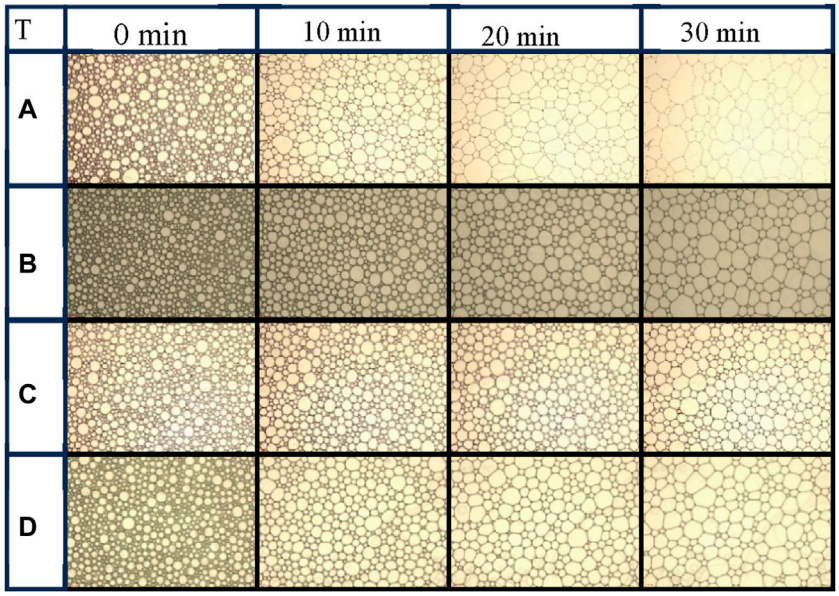

FIGURE 8
The change of foam with time observed by microscope. **(A)** Naked SiO_2, **(B)** 1% KH570@SiO_2, **(C)** 4.77% KH570@SiO_2, **(D)** 7.7% KH570@SiO_2.

3.2 Factors affecting foam ability and stability

3.2.1 Static stability of bulk foams

Foaming was made using the Waring blending with dispersions of SiO_2 or KH570@SiO_2 nanoparticles (0.2wt%) with different contact angles and AOS (0.2wt%). The foam volume and $t_{1/2}$ are presented in Figure 7. The foaming volume and $t_{1/2}$ of the dispersion with naked SNPs were 658 mL and 448 s, respectively. The foaming volume decreased slightly with increasing contact angle, possibly attributed to KH570@SiO_2 being better dispersed and increasing the viscosity of the foaming dispersion. In these experiments, the rate of the blender is 8,000 rpm, which means the energy supplied for foaming is constant. Therefore, the foam volume decreases. The $t_{1/2}$ initially increased first with increasing contact angle and then decreased. When the contact angle of KH570@SiO_2 nanoparticles was around 60°, the $t_{1/2}$ (580 s) at maximum increased by 29.4% which is better than the foam system stabilized by $(CH_3)_2SiCl_2$-modified silica particles (Zhu et al., 2017) compared to the naked SNPs stabilized foam, indicating that the stability of the foam is strongest when the contact angle of KH570@SiO_2 nanoparticles is near 60°. Therefore, when the hydrophilicity and hydrophobicity are too strong, the synergistic effect with the surfactant cannot achieve a moderate hydrophobic effect on the nanoparticle surface. Consequently, the SNPs cannot firmly adsorb at the gas-liquid interface, resulting in ineffective enhancement of foam stability. The properties of the foam are a combination of foaming volume and foam stability, and the effect is optimal when the contact angle of KH570@SiO_2 nanoparticles is around 60°.

Figure 8 illustrates the dynamic changes in the foams stabilized by AOS (0.2wt%)-SiO_2 (0.2wt%) or AOS (0.2wt%)-KH570@SiO_2 (0.2wt%)with different contact angles at 0 min, 10th min, 20th min, and 30th min. Compared to the foam stabilized by naked SNPs (Figure 8A), it is evident that the foam stabilized by KH570@SiO_2 nanoparticles exhibits a slower increase in size (Figures 8B–D). Specifically, after 20 min, the foam stabilized by naked SNPs displays bubbles arranged in a polygonal pattern. These bubbles have larger diameters, resulting in the foam skeleton. In contrast, the foam stabilized by KH570@SiO_2 particles maintains fine textures, particularly for particles with a contact angle of approximately 60° (Figure 8C). The presence of KH570@SiO_2 particles leads to a higher proportion of smaller bubbles and less variability in bubble sizes, suggesting a significant deceleration in foam coalescence. However, as the contact angle of KH570@SiO_2 increases to 90.3°, the coalescence of foam becomes more obvious (Figure 8D, evidenced by a reduction in the number of bubbles and a decrease in roundness at the 20-min mark. These observations align with the findings derived from $t_{1/2}$ measurements conducted on the foam. Figure 9 shows changes in the D_{50} of the foam at the beginning and 20th minute. Initially, the D_{50} of the foam stabilized by naked SNPs is 246 μm. However, D_{50} decreases to 214 μm when the contact angle reaches 60°. This decrease can be explained by the nanoparticles present in the liquid phase aggregating on the surface of the bubbles. Notably, the variation in D_{50} at 20 min aligns with the trends observed in the images.

3.2.2 Mechanism of KH570@SiO_2 nanoparticles stabilization of foam

After grafting -CH_3 onto the surfaces of SNPs, the surfaces become partially hydrophobic, allowing SNPs to adsorb at the gas-liquid interface. To investigate the adsorption of KH570@SiO_2 particles on the gas-liquid surface, the optical microscope experiments were performed first and the microscopic images from generated foams by KH570@SiO_2 nanoparticles (0.2wt %)-AOS (0.2wt%) with a contact angle of 61.5°dispersions were demonstrated in Figure 10. Fluorescence microscopy analysis, as shown in Figure 10B, reveals a distinct visualization of the foam structure stabilized by KH570@SiO_2 particles, compared to foam

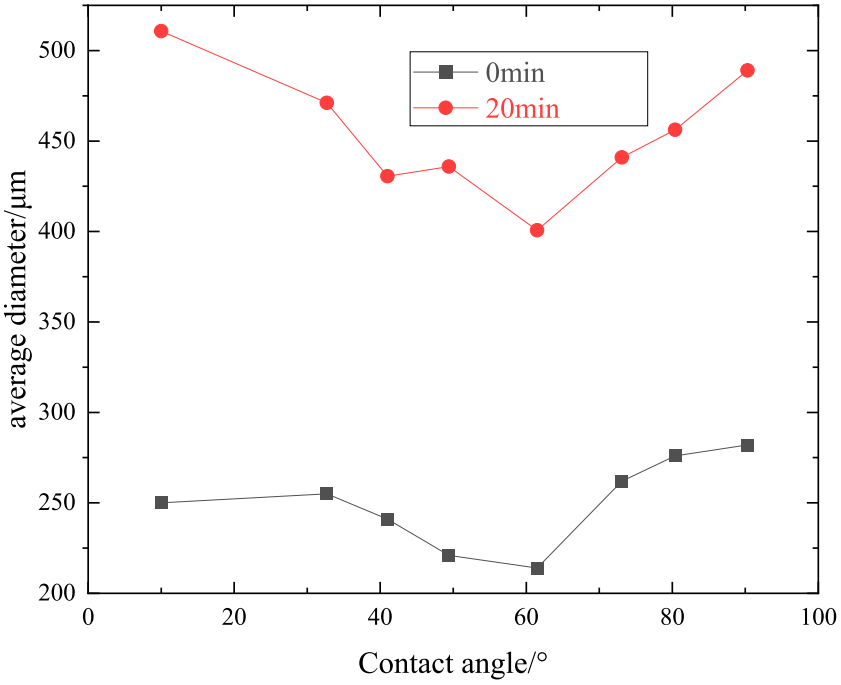

FIGURE 9
Average diameter of bubbles changes with time.

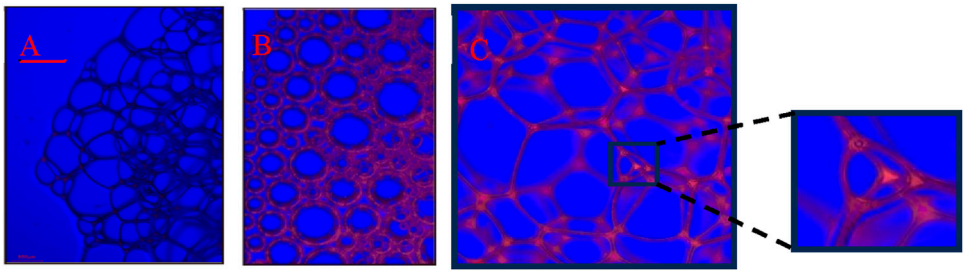

FIGURE 10
Confocal fluorescence image for the foams stabilized only by AOS **(A)** and fluorescently labeled KH570@SiO_2-AOS **(B,C)**. **(B)** Wet foams, **(C)** dry foams.

only stabilized by AOS as illustrated in Figure 10A. The adsorption of KH570@SiO_2 particles onto the gas bubble surfaces, with some particles forming layers separated by platform boundaries, facilitates the formation of a three-dimensional network structure, thereby significantly enhancing foam stability. To visualize the particle distribution more clearly, the liquid from the foam in Figure 10B was drained to form dry foam skeletons, represented in Figures 10C. Notably, some particles are embedded within the dry foam structure, confirming the adhesion of particles to gas bubble surfaces. The retention of particles within the dry foam framework provides evidence that if the particles were in the surrounding continuous phase and not adhering to gas bubble surfaces, they would have been expelled during liquid drainage, rather than being retained within the dry foam skeleton.

3.3 Microscopic displacement characteristics of foam

3.3.1 Study on the flow of foam in microscopic pores

The stability of the foam in the static condition of the microscopic model is given by Guo et al. (2006), and the flow state of the foam stabilized by the modified nanoparticles is described in this experiment. Figure 11 demonstrates the flow of foam in microscopic pores. A comparison is presented between foam generated by KH570@SiO_2 (0.2wt%) with a contact angle of 61.5°and only AOS (0.2wt%) dispersion, and foam generated only by AOS (0.2wt%). Foam stabilized by KH570@SiO_2-AOS, in comparison to foam stabilized by AOS, can keep smaller sizes

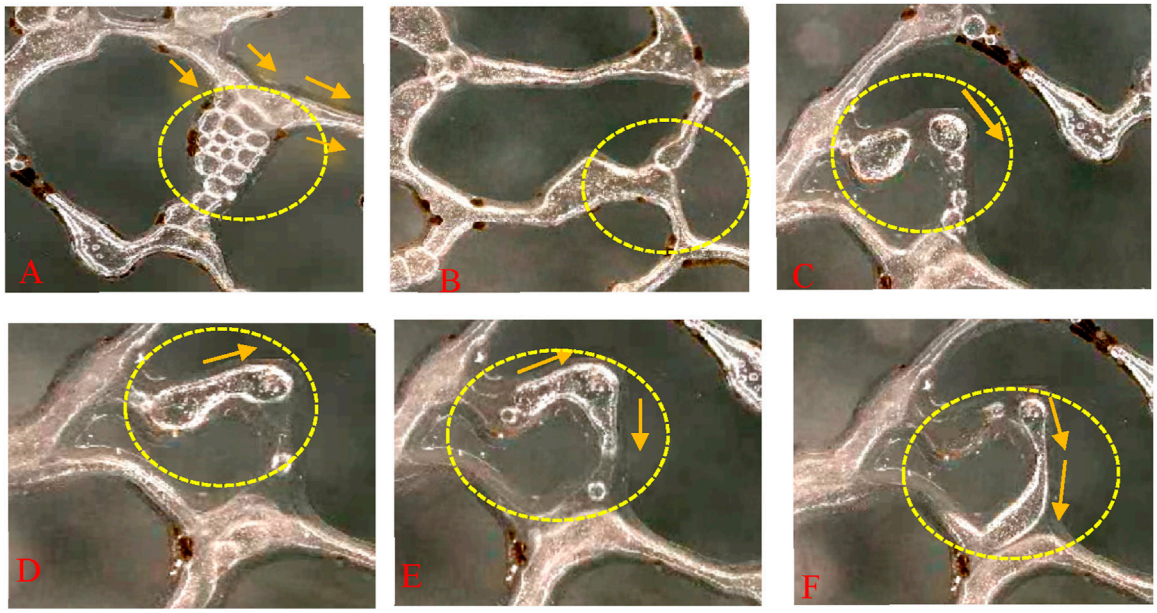

FIGURE 11
The image of flowing characteristics of the foam fluid in porous media **(A,C)** are KH570@SiO_2-AOS foam; **(B,D–F)** are AOS foam.

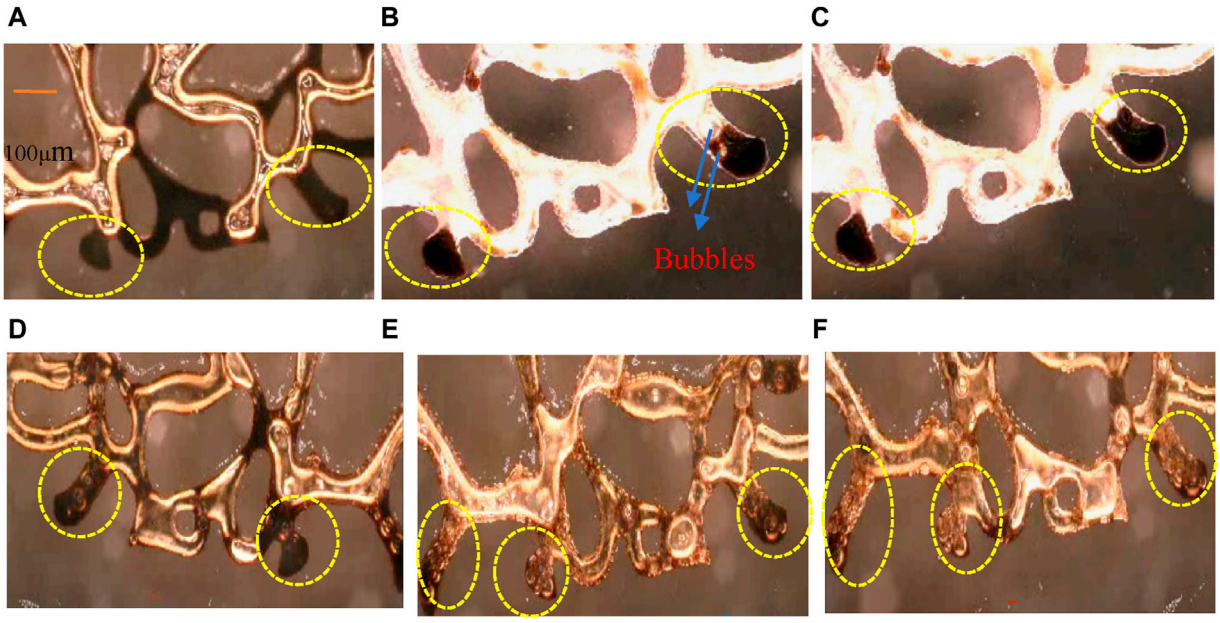

FIGURE 12
Images of residual oil with different displacement phases **(A)** After water flooding, **(B,C)** AOS foam flooding, **(D–F)** Foam stabilized by KH570@SiO_2-AOS flooding.

over a longer period. This is achieved through the formation of bridging blockages with small bubbles and single-bubble blocking up, as Figures 11A, C. The small bubbles aggregate, with liquid films facilitating interactions between neighboring bubbles, leading to enhanced resistance to flow. Consequently, subsequent foam is compelled into narrower channels. Conversely, Figure 11B illustrates the flow of AOS foam, where bubbles amalgamate into larger trains that can go through the pores by deformation without effective blockage. Notably, the slightly larger bubbles formed by KH570@SiO_2-AOS lead to less deformable liquid films due to particle adsorption on the bubble surface. Consequently, it is prone to blockage when passing through a throat, as illustrated in Figure 11C. Contrastingly, in AOS foam, bubbles without soil-absorbed surface are easier to

10.3389/fenrg.2024.1386538

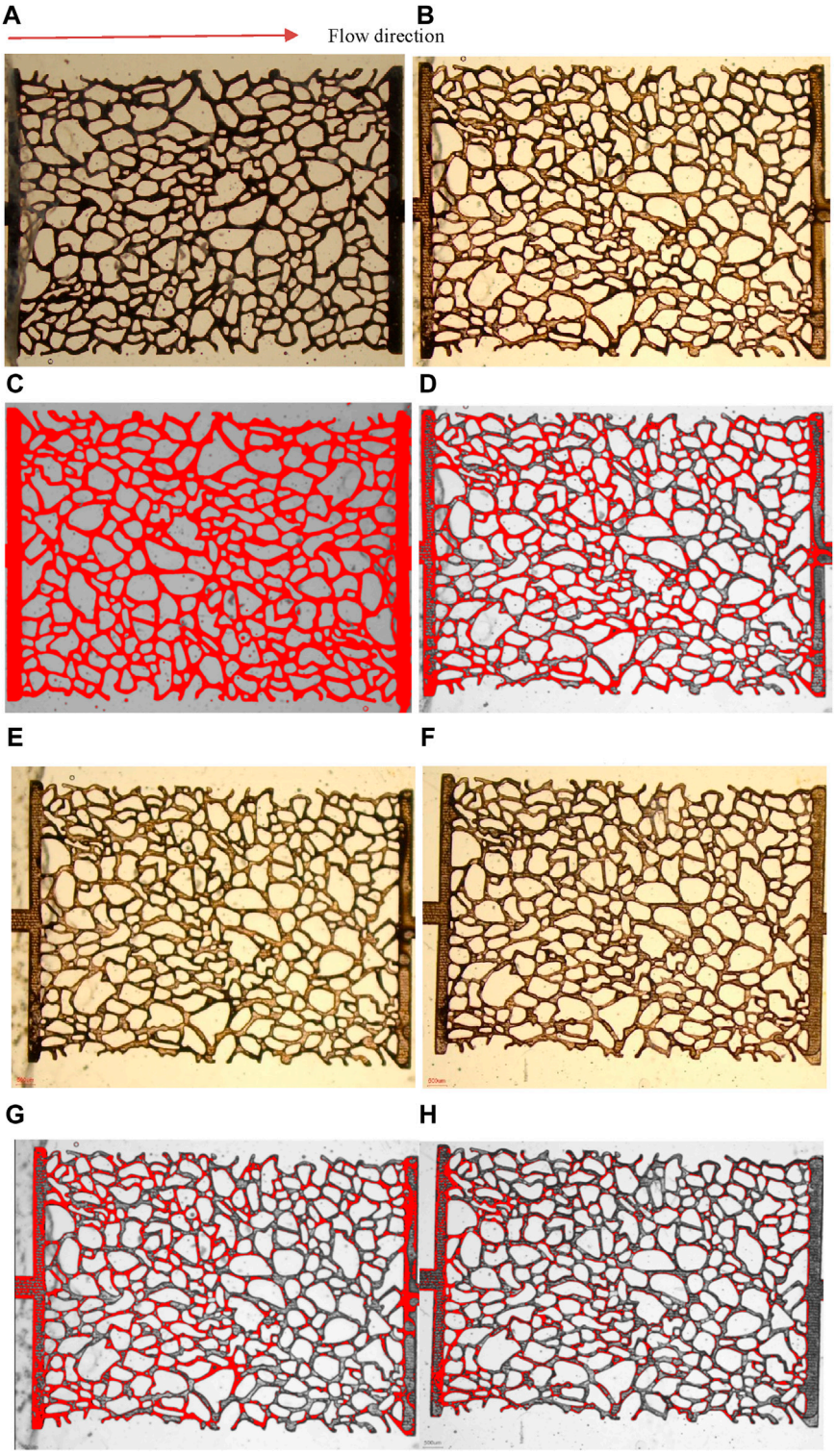

FIGURE 13
Microscopic images of residual oil distributions in 2D micromodel. Figures **(A,B,E,F)** were raw images of initial oil distribution, residual oil distributions after water flooding, AOS foam flooding and extended water flooding, and KH570@SiO_2-AOS foam flooding and extended water flooding respectively, while **(C,D,G,H)** were processed images **(A,B,E,F)** using ImageJ software to estimate trapped oil. Dark brown is oil and milky color is displacement fluids in **(A,B,E,F)** whereas red is oil and ash color is displacement fluid in **(C,D,G,H)**. The flow direction is from left to right.

deform and are more likely to flow through a throat, resulting in ineffective blockages, as evidenced in Figures 11D–F, indicating a weaker blockage.

3.3.2 Micro displacement mechanism

Oil displacement experiments were conducted using AOS (0.2wt%) and KH570@SiO_2 (0.2wt%)-AOS (0.2wt%) foams.

Dead-end pores, very common in rocks, are characterized by only one end connected to the pore-throat network. Upon water flooding, residual oil is distributed in dead-end pores, with the driving force of water proving insufficient to penetrate the higher viscosity dead-end residual oil. This results in residual oil in dead-end pores as depicted in Figure 12A. It is still a great challenge to recover dead-end residual oil. The subsequent AOS foam displacement process, shown in Figures 12B, C, reveals the residual oil in dead-end pores cannot be displaced completely using the foam only stabilized by AOS. The foam stability generated only by AOS is inadequate, with a limited number of small-sized bubbles maintained, and most of the bubble sizes are larger than the throat size, so the larger bubbles are difficult to squeeze into the dead-end pores. Even if smaller AOS bubbles manage to touch the top oil in dead-end pores, they quickly coalesce and enlarge due to poor oil tolerance, preventing further penetration, and leaving some residual oil still in dead-end pores, as illustrated in Figure 12C. In contrast, KH570@SiO_2-AOS foam more effectively displaces residual oil from dead-end pores compared to only AOS foam. Figures 12D–F demonstrate the displacement process by the KH570@SiO_2-AOS foam. The adsorption of particles on the bubble surface enhances interfacial viscoelasticity, thus increasing the foam's blockage capability and facilitating efficient flow channel blockage. KH570@SiO_2-AOS foam stability is superior, maintaining relatively small bubbles for an extended period, reducing flow resistance when entering dead-end pores, and enabling deeper penetration into oil-containing dead-end pores, as illustrated in Figure 12D. Within the dead-end pores, bubbles deform under the influence of driving forces. While AOS bubbles are compressed against the surface of the residual oil due to the high viscosity of oil, KH570@SiO_2-AOS bubbles possess higher interfacial viscoelasticity. Deformed KH570@SiO_2-AOS bubbles tend to restore their original shape, gradually displacing residual oil into a film or droplets and allowing for efficient displacement from the dead-end, as observed in Figure 12E. Ultimately, the majority of oil in the dead-end pores is displaced by the KH570@SiO_2-AOS foam, as shown in Figure 12F. The result indicates that the foam stabilized by the KH570@SiO_2 particles displacement system drives the residual oil in dead-end pores by way of the lots of small bubbles blocking the water channel, enhancing the driving force of the bubble into dead-end pores, then squeezing, deformating, and restorating.

ImageJ software was used to calculate the residual oil in the full microscopic model after different fluid displacements. Figures 13A, C were raw images of initial oil distribution before flooding. The pores of microscopic model is full of oil. In the process of microscopic displacement, water flooding was carried out firstly and then a slug (0.3 PV) of the foam was injected at the residual oil saturation, followed by an extended water flooding. During water flooding, there was a significant "viscous fingering" phenomenon due to the low resistance of the large pores. The injected water preferentially entered into the large pores, and only a small amount of water was driven into the small pores. There is a large amount of residual oil after water flooding, Figures 13B, D. The displacement effects of water flooding, AOS foam flooding, and KH570@SiO_2-AOS were compared (Figure 13). After AOS foam flooding and extend water flooding, there's less residual oil, as shown in Figures 13E, G. However, after KH570@SiO_2-AOS foam flooding and extend water flooding, the distribution of residual oil is further reduced, as shown in Figures 13F, H. The recovery of water flooding, AOS foam flooding, and KH570@SiO_2-AOS was 59.5%, 70.4%, and 79.1% respectively. Less oil was trapped during the KH570@SiO2-AOS and extended water displacement, indicating that KH570@SiO_2-AOS and extended water displacement could achieve the best oil recovery. This system was more effective in mobilizing and displacing residual oil to the production outlet than water flooding and AOS foam flooding followed by water flooding. The displacement behavior is consistent with the pore-scale visualization observations in Figure 12.

4 Conclusion

In summary, KH570@SiO_2 nanoparticles were successfully synthesized by modifying SNPs using KH570. The chemical composition and wettability of KH570@SiO_2 particles were characterized using the equipment. Through the stability experiment of the foam, the modified particles with the optimal contact angle were selected. For the first time, the effect of modified nanoparticles on foam deformation and the microscopic mechanism of enhanced EOR of modified nanoparticle-stabilized foam are demonstrated. The conclusions are as follows:

(1) The successful grafting of coupling agent KH570 onto the surface of SNPs through chemical reactions has been achieved, leading to the effective control of the wettability of the SNPs' surface. The surface hydrophobicity of the modified particles disperses well in AOS solution, reduction of aggregation, and attaining particle size below 100 nm.

(2) The foam stability is effectively improved when the contact angle of particles is approximately 60°. Under the optimum conditions, the drainage half-life increases by 29.4% compared to the foam stabilized by naked SNPs, and the foam displays a finer texture, slower drainage rate, and decreased incidence of bubble coalescence. Through fluorescence microscopy analysis reveal that KH570@SiO2 particles are adsorbed on the liquid film, and the three-dimensional network structure is formed between the armored bubbles, thus the foam stability increases.

(3) Microscopic displacement experiments demonstrate that KH570@SiO_2 with a contact angle close to 60° improved the dynamic stability of foam, forming a bridging blockage with small bubbles and plugging blockage with large bubbles. Compared to the foam stabilized only by AOS, KH570@SiO_2-AOS foam shows higher interfacial viscoelasticity and superior deformation resistance.

(4) The foam stabilized by KH570@SiO_2 nanoparticles can enhance the oil recovery by displacing most of the residual oil in dead-end pores. The stability and swelling viscoelasticity of the foam with KH570@SiO_2 nanoparticles allow the foam to have lots of small bubbles that can block the water channel,

enhancing the driving force of the bubbles enter dead-end pores deeper, then the bubbles are squeezed, deformed, and recovered so that the residual oil in dead-end pores is displaced. KH570@SiO_2 (0.2wt%)-AOS (0.2wt%) foam flooding increased the recovery by 8.7% compared to AOS (0.2wt%) foam flooding.

Data availability statement

The original contributions presented in the study are included in the article/Supplementary material, further inquiries can be directed to the corresponding author.

Author contributions

DY: Data curation, Funding acquisition, Investigation, Methodology, Project administration, Resources, Supervision, Validation, Visualization, Writing–original draft, Writing–review and editing. QL: Formal Analysis, Software, Visualization, Writing–review and editing. DZ: Formal Analysis, Methodology, Software, Validation, Writing–review and editing. TH: Methodology, Resources, Visualization, Writing–review and editing.

Funding

The author(s) declare that financial support was received for the research, authorship, and/or publication of this article. This work has been financially supported by the National Natural Science Foundation of China (Nos 52004247 and 51604243) and Zhoushan Science and Technology Bureau (No. 2021C21024), China Scholarship Council.

Acknowledgments

The authors would like to express their appreciation for the financial support received from the National Natural Science Foundation of China (Nos 52004247 and 51604243) and Zhoushan Science and Technology Bureau (No. 2021C21024), China Scholarship Council, and College of Petrochemical Engineering and Environment of Zhejiang Ocean University for permission to publish this paper.

Conflict of interest

The authors declare that the research was conducted in the absence of any commercial or financial relationships that could be construed as a potential conflict of interest.

Publisher's note

All claims expressed in this article are solely those of the authors and do not necessarily represent those of their affiliated organizations, or those of the publisher, the editors and the reviewers. Any product that may be evaluated in this article, or claim that may be made by its manufacturer, is not guaranteed or endorsed by the publisher.

References

Almubarak, M., Alyousef, Z., Almajid, M., Almubarak, T., and Ng, J. H. (2020). *Enhancing foam stability through a combination of surfactant and nanoparticles. Abu dhabi international petroleum exhibition and conference.*

Bayat, A. E., Rajaei, K., and Junin, R. (2016). Assessing the effects of nanoparticle type and concentration on the stability of CO2 foams and the performance in enhanced oil recovery. *Colloids Surfaces A Physicochem. Eng. Aspects* 511, 222–231. doi:10.1016/j.colsurfa.2016.09.083

Binks, B. P., and Horozov, T. S. (2005). Aqueous foams stabilized solely by silica nanoparticles. *Angew. Chem. Int. Ed.* 44 (24), 3722–3725. doi:10.1002/anie.200462470

Bizmark, N., and Ioannidis, M. A. (2018). Nanoparticle-stabilised emulsions: droplet armouring vs. droplet bridging. *Soft Matter* 14 (31), 6404–6408. doi:10.1039/c8sm00938d

Coates, J. (2000). Interpretation of infrared spectra, a practical approach. *Encycl. Anal. Chem.* 12, 10815–10837. doi:10.1002/9780470027318.a5606

Deschamps, F., Isoardo, T., Denis, S., Tsapis, N., Tselikas, L., Nicolas, V., et al. (2019). Biodegradable Pickering emulsions of Lipiodol for liver trans-arterial chemo-embolization. *Acta Biomater.* 87, 177–186. doi:10.1016/j.actbio.2019.01.054

Du, C., Chang, Z., Yu, H., Zhu, Y., Ma, Y., Ma, G., et al. (2022). Magnetic quantum dots-stabilized foam fluid for enhanced oil recovery. *Chem. Eng. J.* 450, 138334. doi:10.1016/j.cej.2022.138334

Farajzadeh, R., Andrianov, A., and Zitha, P. L. J. (2010). Investigation of immiscible and miscible foam for enhancing oil recovery. *Industrial Eng. Chem. Res.* 49 (4), 1910–1919. doi:10.1021/ie901109d

Gu, Z., Lu, T., Li, Z., and Xu, Z. (2022). Experimental investigation on the SiO2 nanoparticle foam system characteristics and its advantages in the heavy oil reservoir development. *J. Petroleum Sci. Eng.* 214, 110438. doi:10.1016/j.petrol.2022.110438

Guo, Z., Xu, C., Lu, Y., and Zhou, L. (2006). Foamability and stability of foam and means of evaluating. *Chem. Eng.* 127, 51. doi:10.16247/j.cnki.23-1171/tq.2006.04.020

Horozov, T. S. (2008). Foams and foam films stabilised by solid particles. *Curr. Opin. Colloid and Interface Sci.* 13 (3), 134–140. doi:10.1016/j.cocis.2007.11.009

Hu, X., Long, Y., Xuan, G., Wang, Y., Huang, X., Xu, Y., et al. (2023). Optimized hydrophobic magnetic nanoparticles stabilized pickering emulsion for enhanced oil recovery in complex porous media of reservoir. *Front. Energy Res.* 11. doi:10.3389/fenrg.2023.1212664

Hunter, T. N., Wanless, E. J., Jameson, G. J., and Pugh, R. J. (2009). Non-ionic surfactant interactions with hydrophobic nanoparticles: impact on foam stability. *Colloids Surfaces A Physicochem. Eng. Aspects* 347 (1-3), 81–89. doi:10.1016/j.colsurfa.2008.12.027

Kaptay, G. (2003). Interfacial criteria for stabilization of liquid foams by solid particles. *Colloids Surfaces A Physicochem. Eng. Aspects* 230 (1-3), 67–80. doi:10.1016/j.colsurfa.2003.09.016

Khajehpour, M., Reza Etminan, S., Goldman, J., Wassmuth, F., and Bryant, S. (2018). Nanoparticles as foam stabilizer for steam-foam process. *SPE J.* 23 (06), 2232–2242. doi:10.2118/179826-pa

Khandoozi, S., Pourafshary, P., Aidarova, S., and Sharipova, A. (2023). A comparative analysis of the effect of nanoparticles/surfactant assisted foam injection on the gas mobility control at different heterogeneities. *Fuel* 350, 128810. doi:10.1016/j.fuel.2023.128810

Khristov, K. I., Exerowa, D., and Krugljakov, P. (1983). Influence of the type of foam films and the type of surfactant on foam stability. *Colloid Polym. Sci.* 261, 265–270. doi:10.1007/bf01469674

Li, R. F., Yan, W., Liu, S., Hirasaki, G. J., and Miller, C. A. (2008). *Foam mobility control for surfactant EOR. SPE symposium on improved oil recovery*. Tulsa, Oklahoma, USA: SPE.

Linke, C., and Drusch, S. (2018). Pickering emulsions in foods-opportunities and limitations. *Crit. Rev. food Sci. Nutr.* 58 (12), 1971–1985. doi:10.1080/10408398.2017.1290578

Maestro, A., Rio, E., Drenckhan, W., Langevin, D., and Salonen, A. (2014). Foams stabilised by mixtures of nanoparticles and oppositely charged surfactants: relationship between bubble shrinkage and foam coarsening. *Soft Matter* 10 (36), 6975–6983. doi:10.1039/c4sm00047a

Mingming, L., and Shuzhong, W. (2014). Stability of carbon dioxide foam and effect of polymer on its foam properties. *J. Chem. Industry Eng. (China)* 65 (6), 2219–2223.

Ojea-Jiménez, I., Urbán, P., Barahona, F., Pedroni, M., Capomaccio, R., Ceccone, G., et al. (2016). Highly flexible platform for tuning surface properties of silica nanoparticles and monitoring their biological interaction. *ACS Appl. Mater. Interfaces* 8 (7), 4838–4850. doi:10.1021/acsami.5b11216

Pieranski, P. (1980). Two-dimensional interfacial colloidal crystals. *Phys. Rev. Lett.* 45, 569–572. doi:10.1103/physrevlett.45.569

Pozrikidis, C. (2001). Numerical investigation of the effect of surfactants on the stability and rheology of emulsions and foam. *J. Eng. Math.* 41 (2/3), 237–258. doi:10.1023/a:1011932500831

Qi, J., Yu, Z. L., Liao, G. P., Luo, Z. Y., and Bai, B. F. (2021). Effect of nanoparticle surfactants on droplet formation in a flow-focusing microchannel. *Phys. Fluids* 33 (11). doi:10.1063/5.0070186

Rezaee, M., Hosseini-Nasab, S. M., Fahimpour, J., and Sharifi, M. (2022). New Insight on improving foam stability and foam flooding using fly-ash in the presence of crude oil. *J. Petroleum Sci. Eng.* 214, 110534. doi:10.1016/j.petrol.2022.110534

Santini, E., Krgel, J., Ravera, F., Liggieri, L., and Miller, R. (2011). Study of the monolayer structure and wettability properties of silica nanoparticles and CTAB using the Langmuir trough technique. *Colloids Surfaces A Physicochem. Eng. Aspects* 382 (1), 186–191. doi:10.1016/j.colsurfa.2010.11.042

Shi, W., Ma, Y., Tao, L., Zhang, N., Ma, C., Bai, J., et al. (2023). Study of the enhanced oil recovery mechanism and remaining oil state of heavy oil after viscosity-reducer-assisted CO2 foam flooding: 2D microvisualization experimental case. *Energy and Fuels* 37 (23), 18620–18631. doi:10.1021/acs.energyfuels.3c03212

Sie, C. Y., and Nguyen, Q. P. (2020). A pore-scale experimental study of non-aqueous foam for improving hydrocarbon miscible flooding. *J. Petroleum Sci. Eng.*, 195. doi:10.1016/j.petrol.2020.107888

Singh, A., Eken, T., Mohanty, D., Saikia, D., Singh, C., and Ravi Kumar, M. (2016). Significant seismic anisotropy beneath southern Tibet inferred from splitting of direct S-waves. *Phys. Earth Planet. Interiors* 250, 1–11. doi:10.1016/j.pepi.2015.11.001

Singh, R., and Mohanty, K. K. (2017). Foam flow in a layered, heterogeneous porous medium: a visualization study. *Fuel* 197, 58–69. doi:10.1016/j.fuel.2017.02.019

Smith, B. C. (2018). *Infrared spectral interpretation: a systematic approach*. CRC Press.

So, B. B. L., and Lumsdon, S. O. (2000). Influence of particle wettability on the type and stability of surfactant-free emulsions. *Langmuir ACS J. Surfaces Colloids* 16 (23), 8622–8631. doi:10.1021/la000189s

Sun, L., Wang, B., Pu, W., Yang, H., and Shi, M. (2015). The effect of foam stability on foam flooding recovery. *Petroleum Sci. Technol.* 33 (1), 15–22. doi:10.1080/10916466.2014.922100

Sun, Q., Li, Z., Li, S., Jiang, L., Wang, J., and Wang, P. (2014). Utilization of surfactant-stabilized foam for enhanced oil recovery by adding nanoparticles. *Energy and Fuels* 28 (4), 2384–2394. doi:10.1021/ef402453b

Wang, B. A. (2014). *Laboratory investigation on influences of three polymers to foam stability at elevated temperature*. Dissertations and Theses - Gradworks.

Wang, C., and Li, H. A. (2016). Stability and mobility of foam generated by gas-solvent/surfactant mixtures under reservoir conditions. *J. Nat. Gas Sci. Eng.* 34, 366–375. doi:10.1016/j.jngse.2016.06.064

Wang, L., Cheng, Y. P., Xu, C., An, F. H., Jin, K., and Zhang, X. l. (2013). The controlling effect of thick-hard igneous rock on pressure relief gas drainage and dynamic disasters in outburst coal seams. *Nat. Hazards* 66 (2), 1221–1241. doi:10.1007/s11069-012-0547-0

Wang, Y., Wang, J., Fan, H., Du, F., Zhou, W., and Yang, J. (2020). Effect of inorganic salt on foam properties of nanoparticle and surfactan systems. *Tenside Surfactants Deterg. J. Theory, Technol. Appl. Surfactants* (5), 57. doi:10.3139/113.110698

Xie, W., Li, X., Chen, Z., and Hui, X. (2007). Review of exploration and development technologies for heavy oil and high pour-point oil in Liaohe oil region. *Shiyou Xuebao/Acta Pet. Sin.* 28 (4), 145–150.

Yao, C., Lei, G., Li, L., and Gao, X. (2012). Selectivity of pore-scale elastic microspheres as a novel profile control and oil displacement agent. *Energy and Fuels* 26 (8), 5092–5101. doi:10.1021/ef300689c

Yousef, Z. A. A., Almobarky, M., and Schechter, D. S. (2017). Enhancing the stability of foam by the use of nanoparticles. *Energy and Fuels* 31 (10), 10620–10627. doi:10.1021/acs.energyfuels.7b01697

Zhao, G., Wang, X., Dai, C., Sun, N., Liang, L., Yang, N., et al. (2021a). Investigation of a novel enhanced stabilized foam: nano-graphite stabilized foam. *J. Mol. Liq.* (343-), 343. doi:10.1016/j.molliq.2021.117466

Zhao, J., Torabi, F., and Yang, J. (2021b). The synergistic role of silica nanoparticle and anionic surfactant on the static and dynamic CO2 foam stability for enhanced heavy oil recovery: an experimental study. *Fuel* 287, 119443. doi:10.1016/j.fuel.2020.119443

Zhu, Q., Zhou, H. L., Song, Y. X., Chang, Z. D., and Li, W. J. (2017). Modification and investigation of silica particles as a foam stabilizer. *Int. J. Minerals Metallurgy Mater.* 24 (2), 208–215. doi:10.1007/s12613-017-1397-2